arXiv:0802.2363v1 [astro-ph] 18 Feb 2008

VERITAS Observations of the γ-ray Binary LS I +61 303

V.A. Acciari[20,1], M. Beilicke[2], G. Blaylock[3], S.M. Bradbury[4], J.H. Buckley[2], V. Bugaev[2], Y. Butt[24], K.L. Byrum[5], O. Celik[6], A. Cesarini[1,21], L. Ciupik[7], Y.C.K. Chow[6], P. Cogan[12], P. Colin[11], W. Cui[8], M.K. Daniel[4], C. Duke[16], T. Ergin[3], A.D. Falcone[22], S.J. Fegan[6], J.P. Finley[8], P. Fortin[14], L.F. Fortson[7], D. Gall[8], K. Gibbs[1], G.H. Gillanders[21], J. Grube[4], R. Guenette[12], D. Hanna[12], E. Hays[5,1], J. Holder[23], D. Horan[5], S.B. Hughes[2], C.M. Hui[11], T.B. Humensky[10], P. Kaaret[18], D.B. Kieda[11], J. Kildea[1], A. Konopelko[8], H. Krawczynski[2], F. Krennrich[9], M.J. Lang[21], S. LeBohec[11], K. Lee[2], G. Maier[12,*], A. McCann[12], M. McCutcheon[12], J. Millis[8], P. Moriarty[20], R. Mukherjee[14], T. Nagai[9], R.A. Ong[6], D. Pandel[18], J.S. Perkins[1], F. Pizlo[8], M. Pohl[9], J. Quinn[13], K. Ragan[12], P.T. Reynolds[19], H.J. Rose[4], M. Schroedter[9], G.H. Sembroski[8], A.W. Smith[1,4], D. Steele [7], S.P. Swordy[10], J.A. Toner[1,21], L. Valcarcel[12], V.V. Vassiliev[6], R. Wagner[5], S.P. Wakely[10], J.E. Ward[13], T.C. Weekes[1], A. Weinstein[6], R.J. White[4], D.A. Williams[17], S.A. Wissel[10], M. Wood[6], B. Zitzer[8]

ABSTRACT

LS I +61 303 is one of only a few high-mass X-ray binaries currently detected

---

[*] Corresponding author: gernot.maier@mcgill.ca

[1] Fred Lawrence Whipple Observatory, Harvard-Smithsonian Center for Astrophysics, Amado, AZ 85645, USA

[2] Department of Physics, Washington University, St. Louis, MO 63130, USA

[3] Department of Physics, University of Massachusetts, Amherst, MA 01003-4525, USA

[4] School of Physics and Astronomy, University of Leeds, Leeds LS2 9JT, UK

[5] Argonne National Laboratory, 9700 S. Cass Avenue, Argonne, IL 60439, USA

[6] Department of Physics and Astronomy, University of California, Los Angeles, CA 90095, USA

[7] Astronomy Department, Adler Planetarium and Astronomy Museum, Chicago, IL 60605, USA

[8] Department of Physics, Purdue University, West Lafayette, IN 47907, USA

[9] Department of Physics and Astronomy, Iowa State University, Ames, IA 50011, USA

[10] Enrico Fermi Institute, University of Chicago, Chicago, IL 60637, USA

[11] Physics Department, University of Utah, Salt Lake City, UT 84112, USA

[12] Physics Department, McGill University, Montreal, QC H3A 2T8, Canada

[13] School of Physics, University College Dublin, Belfield, Dublin, Ireland

[14] Department of Physics and Astronomy, Barnard College, Columbia University, NY 10027, USA

[16] Department of Physics, Grinnell College, Grinnell, IA 50112-1690, USA

[17] Santa Cruz Institute for Particle Physics and Department of Physics, University of California, Santa Cruz, CA 95064, USA

[18] Department of Physics and Astronomy, University of Iowa, Van Allen Hall, Iowa City, IA 52242, USA

[19] Department of Applied Physics and Instrumentation, Cork Institute of Technology, Bishopstown, Cork, Ireland

[20] Department of Life and Physical Sciences, Galway-Mayo Institute of Technology, Dublin Road, Galway, Ireland

[21] Physics Department, National University of Ireland, Galway, Ireland

[22] Department of Astronomy and Astrophysics, Penn State University, University Park, PA 16802, USA

[23] Department of Physics and Astronomy, Bartol Research Institute, University of Delaware, Newark, DE 19716, USA

[24] Smithsonian Astrophysical Observatory, Cambridge, MA 02138, USA

at high significance in very high energy γ-rays. The system was observed over several orbital cycles (between September 2006 and February 2007) with the VERITAS array of imaging air-Cherenkov telescopes. A signal of γ-rays with energies above 300 GeV is found with a statistical significance of 8.4 standard deviations. The detected flux is measured to be strongly variable; the maximum flux is found during most orbital cycles at apastron. The energy spectrum for the period of maximum emission can be characterized by a power law with a photon index of $\Gamma = 2.40 \pm 0.16_{stat} \pm 0.2_{sys}$ and a flux above 300 GeV corresponding to 15-20% of the flux from the Crab Nebula.

Subject headings: gamma rays; LS I +61 303; X-ray binary; acceleration of particles

LS I +61 303.

1. Introduction

The high-mass X-ray binary LS I +61 303 consists of a massive Be-type star surrounded by a dense circumstellar disk (Hutchings & Crampton 1981; Gregory & Neish 2002) and a compact object. It has recently been detected as a source of very high energy (VHE) γ-rays by the MAGIC telescope (Albert et al. 2006) and confirmed by VERITAS (Maier et al. 2007). This increases the number of γ-ray binaries to three; the other two are PSR B1259-63 (Aharonian et al. 2005) and LS 5039 (Aharonian et al. 2006a). While the γ-ray emission in PSR B1259-63 is powered by the relativistic wind of the young 48-ms pulsar, the unknown nature of the compact objects in LS I +61 303 and LS 5039 does not exclude microquasar-type emission models. These X-ray binary systems provide unique laboratories for studying particle acceleration by providing detailed information about the time-evolution of the particle spectrum over the orbital period.

Optical and radio observations of LS I +61 303 show that the compact object orbits the massive star every 26.496 days; the elliptical orbit is characterized by a semi-major axis of only a few stellar radii and an eccentricity of 0.72 ± 0.15 (Casares et al. 2005; Grundstrom et al. 2007). The distance to LS I +61 303 is approximately 2 kpc (Steele et al. 1998). The radio, optical and X-ray emission of the binary has a component which is clearly modulated at the orbital period (Taylor & Gregory 1982; Mendelson & Mazeh 1989; Leahy 2001; Wen et al. 2006; Smith et al. 2007), although considerable variation in the lightcurve is observed from orbit to orbit (e.g. Sidoli et al. (2006)). Orbital modulation in low-energy (>100 MeV) or high-energy γ-rays (>300 GeV) is not yet confirmed (Massi

2004; Albert et al. 2006). An association of LS I +61 303 with the COS-B γ-ray source 2CG 135+01 (Swanenburg et al. 1981) was proposed early on (Taylor & Gregory 1978), and observations with EGRET (3EG J0241+6103) for photon energies >100 MeV supported this (Kniffen et al. 1997). The MAGIC observations in VHE γ-rays provided the first firm connection of the site of the variable very-high energy γ-ray emission with LS I +61 303.

This paper reports on stereoscopic observations of LS I +61 303 with the ground-based γ-ray observatory VERITAS, at energies above 300 GeV. A publication describing contemporaneous X-ray and TeV observations is in preparation (Acciari et al. 2008). We adopt orbital parameters as derived from radio data by Gregory (2002) with an orbital period of $P = 26.4960 \pm 0.0028$ days and zero orbital phase of T_0 = HJD 2443366.775. The periastron takes place at phase 0.23, apastron is at phase 0.73, and inferior and superior conjunctions are at phases 0.26 and 0.16 respectively (Casares et al. 2005).

2. Observations and analysis

The observations of LS I +61 303 were made between September 2006 and February 2007 during the construction phase of VERITAS, an array of four 12-m imaging Cherenkov telescopes. VERITAS is located at the basecamp of the Fred Lawrence Whipple Observatory in southern Arizona (1268 m a.s.l., $31^{\circ}40'30''$N, $110^{\circ}57'07''$W, Weekes et al. (2002)). The system combines a large effective area ($> 3 \times 10^4$ m^2) over a wide energy range (100 GeV to 30 TeV) with good energy (10-20%) and angular resolution ($< 0.14^{\circ}$ on an event-by-event basis).

The overall design of all four VERITAS telescopes is identical. Each telescope employs a 12 m-diameter tessellated mirror of Davies-Cotton design (Davies & Cotton 1957) with 12 m focal length, mounted on a altitude-over-azimuth positioner. The reflector comprises 350 hexagonal mirror facets giving a total mirror area of 106 m^2. The focal plane is equipped with a 499-element photomultiplier-tube (PMT) imaging camera. The angular pixel spacing is 0.15°, giving a field of view of 3.5°. Light cones installed in front of the cameras increase the photon collection efficiency and shield the PMTs from ambient light. The three-level trigger system of the VERITAS array allows a substantial suppression of background events at the trigger level. It especially suppresses events due to local muons which are a considerable background in single-telescope operation. The first level of the trigger system consists of custom built constant fraction discriminators (CFD), one for each PMT. All observations described here were made with a CFD threshold of 50 mV, corresponding to approximately 4-5 photoelectrons. The second level, a pattern trigger, requires at least three adjacent triggered pixels in order to generate a camera trigger. The array trigger determines if level-two triggers from individual telescopes are consistent with an air shower. A coincidence of at least two telescopes triggering within a time window of 100 ns is required. When the array is triggered, PMT signals in each telescope are digitized using 500 Megasample/second custom-built flash-ADC electronics. To achieve a large dynamic range, an autoranging gain switch extends the dynamic range from 256 to 1500. In the event of a telescope trigger, all signals (i.e. a 48 ns long flash-ADC trace) from all channels in all telescopes are read out as a stereo event. A description of the technical details and the performance of VERITAS can be found in (Holder et al. 2006; Maier et al. 2007) and references therein.

Observations of LS I +61 303 with VERITAS were made with different configurations as the array construction proceeded; no changes to the individual telescopes were implemented in this period. Observations from September 2006 to November 2006 were made with a two-telescope system while those for January and February 2007 were made with three telescopes. The typical array trigger rate was 90 events/s for the two-telescope system (with a dead time of 4%), and 160 events/s (7% dead time) for the three-telescope system. Data were taken on moonless nights in "wobble-mode", wherein the source was positioned at a fixed offset from the camera center. This has the advantage that no off-source observations are necessary for background estimation. The conservative energy threshold after the analysis cuts adopted here is 300 GeV at 30^{o} zenith angle. The dataset consists of 45.9 hours of observations after quality cuts and dead-time corrections. The quality cuts remove all data taken under non-optimal conditions (e.g. bad weather, runs with large trigger-rate fluctuations, runs with malfunction of the telescope system). There is good coverage of LS I +61 303 for orbital phases from 0.4 to 0.9, but since observations were precluded by the bright moon, no observations were possible during orbital phases from 0.9 to 0.2. Table 1 shows the most important observational parameters for each of the five observation periods.

The first step in the analysis is the calibration and integration of the flash-ADC traces, as described in detail in (Holder et al. 2006). The calibration is divided into several sections. The absolute calibration uses a laser system in order to determine the signal size produced by single photons. In the relative calibration, laser events are used to calculate the relative gains of the pixels and timing differences due to path length differences in the cabling of each channel. Pedestal events, injected at 1 Hz during an observation run, are used for an estimation of the voltage offset in each flash-ADC trace and the noise levels due to the night sky background and electronics. The amount of charge in each flash-ADC trace is calculated by summing the samples for a given window size. A two-pass summation method is used here, allowing the integration of the flash-ADC traces with an optimal signal-to-noise ratio. The resulting image of an air shower is cleaned in order to remove pixels which contain mainly background light. The cleaning consists of a two-level filter removing all pixels with an integrated charge smaller than 5 times their pedestal standard deviation and any pixel that are adjacent to these higher threshold pixels and having signals smaller than 2.5 times their pedestal standard deviation. The shower image is then parameterized with a second moment analysis (Hillas 1985). The direction of origin of the γ-ray on the sky and the impact parameter of the shower core on the ground are reconstructed using stereoscopic techniques (Hofmann et al. 1999; Krawczynski et al. 2006). At least two images with an integrated charge per image > 400 digital counts ($\approx$75 p.e.) and a maximum image distance from the center of the camera of less than 1.2° are required in this reconstruction stage. The majority of the far more numerous background events are rejected by comparing the shape (i.e. width and length) of the event images in each telescope with the expected shapes of γ-ray showers modeled by Monte Carlo simulations. These so-called *mean-scaled width* and *mean-scaled length* parameters (Konopelko 1995; Krawczynski et al. 2006) are calculated with lookup tables based on Monte Carlo simulations. The lookup tables contain the median and 90%-widths of the image parameter width (w_{MC}, $\sigma_{width,MC}$) and length (l_{MC}, $\sigma_{length,MC}$) as a function of impact parameter R, integrated charge per image s, and zenith angle Θ:

$$mscw = \frac{1}{N_{Images}} \left(\sum_{i}^{N_{Images}} \frac{width_i - w_{MC}(R, s, \Theta)}{\sigma_{width,MC}(R, s, \Theta)} \right)$$

and similar for mean scaled length. The cuts applied here are $-1.2 <$ mean scaled width/length < 0.5 and reconstructed distance of shower core position from the center of the array $<$ 250 m. This and an additional cut on the arrival direction of the incoming γ-ray ($\Theta^2 < 0.025$ deg^2) reject more than 99.9% of the cosmic-ray background while keeping 45% of the γ-rays. All the cuts are optimized a priori with Monte Carlo simulations of γ-ray- and hadron-induced air showers. The background in the source region is estimated from the same field of view using the "reflected-region" model and the "ring-background" model as described in Berge et al. (2007).

The energy of each event in the source and background region is estimated from Monte Carlo simulations assuming that the primary particle is a γ-ray. The calculation uses lookup tables and determines the energy of an event as a function of impact parameter, integrated charge per image, and zenith angle. Collection areas at different zenith angles for γ-rays are produced from Monte Carlo simulations following (Mohanty et al. 1998); collection areas are interpolated between zenith angle bins to the zenith angle of each event. The limited energy resolution is taken into account by calculating the collection areas as a function of reconstructed energy. The differential flux dN/dE in each energy bin of width ΔE is then calculated with the number of events in the source region (N_{source}) and in the background region (N_{bck}), the ratio of the size of the source region to the size of the background region

(α), the dead time corrected observation time T, and the collection area A:

$$dN/dE = \left(\sum_{i=1}^{N_{source}} 1/A_i - \alpha \sum_{i=1}^{N_{bck}} 1/A_i \right) /T/\Delta E$$

The dependence of the collection area on the spectral index is taken into account by an iterative process. In each step of the iteration, collection areas are calculated using the spectral index obtained in the previous step. The iteration stops when convergence is achieved, usually after 2-3 steps. In order to accurately calculate source fluxes and energy spectra, a model of the telescope response to air showers has been developed. The Monte Carlo simulations take all relevant processes and efficiencies in the development of the air shower through the atmosphere, the propagation of Cherenkov photons through the optical system of the telescopes, and the response of the camera and electronics into account; see (Holder et al. 2006) for more details. The systematic error in the energy estimation is dominated by uncertainties and variabilities of the atmospheric conditions, in the Monte Carlo simulations, and in the overall photon collection efficiency.

3. Results

We have detected LS I +61 303 as a source of γ-rays with energies above 300 GeV, at a total significance of 8.4 σ at the position of the optical counterpart. The source has been found to be variable, as earlier measurements by MAGIC suggest. The probability that the measured fluxes from LS I +61 303 are constant with time or orbital phase has been determined with a χ^2-test to be less than $\sim 10^{-9}$. The two-dimensional sky map of significances for the region around LS I +61 303 shows a strong detection for orbital phases 0.5-0.8, i.e., around apastron (Figure 1). No signal has been found for orbital phases 0.8-0.5. The position of the peak of the γ-ray emission, reconstructed by a fit to the uncorrelated map of excess events with a two-dimensional normal distribution, is in agreement with the position of the optical source: $\Delta_{\rm RA} = 147 \pm 73_{\rm stat}$ arcsec, $\Delta_{\rm dec} = -34 \pm 30_{\rm stat}$ arcsec (corresponding to $\mathrm{RA}_{\rm J2000}$ $2^{\rm h}40^{\rm m}41^{\rm s}$, $\mathrm{Dec}_{\rm J2000}$ $61^{\rm o}13'12''$). The systematic uncertainty is ±90 arcseconds[1]. This is consistent with the position of the TeV excess reported by MAGIC. The morphology of the excess is compatible with the expected distribution due to a point source. The VERTIAS source name is VER J0240+612.

In Figure 2 we show the differential energy spectrum during the high-flux phases 0.5-0.8

---

[1] There were no optical pointing monitors installed during these observations with the array under construction. The pointing accuracy is expected to improve to <15 arcsec for the completed system.

for γ-ray energies between 300 GeV and 5 TeV. The integrated flux of VHE photons in this energy range is $(8.13 \pm 1.02) \times 10^{-12}$ cm^{-2}s^{-1}. The shape is consistent with a power law $\mathrm{dN/dE} = \mathrm{C}\times(\mathrm{E}/1\ \mathrm{TeV})^{-\Gamma}$ with a photon index $\Gamma = 2.40 \pm 0.19_{stat} \pm 0.2_{sys}$ and a flux normalization constant $\mathrm{C} = (2.89 \pm 0.32_{stat} \pm 0.6_{sys}) \times 10^{-12}$ cm^{-2}s^{-1}TeV^{-1}. The χ^2 of the fit is 2.1 for 5 degrees of freedom.

The dependency of integral fluxes on orbital phase (Figure 3) shows that significant fluxes above 2σ are only detected during orbital phases close to apastron. Peak fluxes measured at phases between 0.6 and 0.8 correspond to 10-20% of the flux of the Crab Nebula, but appear to vary from one orbital cycle to the next. Upper limits in a range corresponding to 3-10% of the flux of the Crab Nebula have been derived for phases 0.3 to 0.6 and around 0.9. The upper limit calculation assumes a similar shape for the energy spectra of TeV γ-rays during all phases. This may not be correct, as the phase-dependent shape of the energy spectra of the X-ray binary LS 5039 shows (Aharonian et al. 2006b). Furthermore, the combination of data from different orbital cycles in Figure 3 (bottom) assumes implicitly that the position of the emission maximum in orbital phase and its flux do not vary from one cycle to the next. A constant maximum γ-ray flux is not necessarily expected; LS I +61 303 shows variable X-ray fluxes over different orbits (e.g. Chernyakova et al. 2006). The VERITAS measurement can neither confirm nor refute this at this stage. The same periodicity for radio and γ-ray data was assumed during this analysis (P=26.4960 days). This has been tested using Lomb-Scargle statistics (Scargle 1982), but large gaps in data taking due to bright moon periods and the periodicity of the observation cycles do not allow definite conclusions.

4. Discussion and Conclusions

LS I +61 303 has been detected in γ-rays at phases around 0.6 to 0.8 only, when the distance between the two objects in the binary system is largest. This indicates a strong dependence of particle acceleration and energy loss mechanisms on the relative positions.

It is suggested that TeV γ-rays are produced in LS I +61 303 in leptonic (inverse Compton scattering of low-energy photons from the stellar companion or pair cascades, see e.g. Bednarek (2006); Gupta & Böttcher (2006)) and/or hadronic interactions (e.g. Romero et al. (2005)). Both production mechanisms require a population of high-energy particles and a sufficiently dense photon field or target material. This is provided abundantly in LS I +61 303 for all orbital phases by stellar photons and the wind of the companion star. Target density is highest around periastron, which favors a maximum in γ-ray emission when the compact object passes close to the stellar companion. The maximum electron energy available for

γ-ray production is, on the other hand, restricted by cooling through inverse Compton and synchrotron emission; both of these effects can be strongest around periastron. In addition, γ-rays emitted too close to the massive star suffer from photon-photon absorption in the dense stellar radiation field. Significant inhomogeneities in the stellar wind can further complicate the process of γ-ray production (Neronov & Chernyakova 2007; Romero et al. 2007b).

The unknown nature of the compact object (neutron star or black hole) allows two very different scenarios to provide the necessary power for the production of VHE γ-rays. In the microquasar model, charged particles (electrons or hadrons) are accelerated in an accretion-driven relativistic jet (Taylor & Gregory 1984; Mirabel & Rodriguez 1994). Acceleration can take place all along the jet or in shocks created in the jet termination zone (Heinz & Sunyaev 2002). The efficiency of particle acceleration and γ-ray production varies over the orbit due to changes in target density, accretion rate, and magnetic field strength. The second scenario assumes that the compact object is a pulsar. Particles are accelerated in the shock created by the collision of the expanding pulsar wind with the equatorial disk or wind of the companion star (Maraschi & Treves 1981), similar to the binary system PSR B1259-63. The distance of the pulsar wind termination shock changes with orbital motion (Dubus 2006). Electron cooling through synchrotron emission is in this model lowest around apastron, when the shock is furthest away from the pulsar and therefore the magnetic field is weakest. This results, under the assumption that enough target photons are available for inverse Compton scattering, in the observed maximum of the γ-ray emission at apastron. More measurements, especially contemporaneous multiwavelength observations are necessary for constraining tests of the available models.

The measured integral flux of γ-rays above 300 GeV in the phase interval 0.6 to 0.8 corresponds to an isotropic luminosity of roughly 10^{34} ergs/s at 2 kpc. The necessary power could either be provided by a pulsar with spindown luminosity of $\sim 10^{36}$ erg/s or by accretion, which has been estimated to be in the range of several 10^{37} erg/s (Romero et al. 2007a). Both scenarios imply conversion factors to γ-ray emission below 1%.

If we compare the average TeV flux with the average GeV flux measured by EGRET (Kniffen et al. 1997), we find a GeV/TeV photon flux ratio of 10^5 which is consistent with that produced by a power-law with photon index 2.4, similar to the photon indexes measured in the two bands. This result should be treated with caution since the source is known to exhibit long-term variability (Gregory 1989) and the measurements are separated by more than 10 years. However, it may suggest that a single power-law could suffice to describe the GeV/TeV spectrum - a possibility that can be tested with future simultaneous GeV/TeV observations.

In conclusion, new stereoscopic observations with VERITAS have confirmed very-high-energy γ-ray emission from LS I +61 303. The source is detected only during orbital phases 0.6 to 0.8, which is close to apastron. This suggests variability connected to the orbital movement, but a definite conclusion has to wait for further measurements. Future observations with the much more sensitive full VERITAS array will allow us to study the VHE emission during the whole orbital cycle.

This research is supported by grants from the U.S. Department of Energy, the National Science Foundation, the Smithsonian Institution, by NSERC in Canada, by Science Foundation Ireland and by PPARC in the UK. We acknowledge the excellent work of the technical support staff at the FLWO and the collaborating institutions in the construction and operation of the instrument.

REFERENCES

Acciari, V. et al.(VERITAS collaboration) 2008, in preparation

Aharonian F. et al. 2005, A&A, 442, 1

Aharonian F. et al. 2006a, Science, 309, 746

Aharonian F. et al. 2006b, A&A, 460, 743

Albert J. et al. 2006, Science, 312, 1771

Bednarek, W. 2006, MNRAS, 371, 1737

Berge, D. et al. 2007, A&A, 466, 1219

Casares J. et al. 2005, MNRAS, 360, 1105

Chernyakova, M. et al. 2006, MNRAS, 372, 1585

Davies, J.M. & Cotton, E.S. 1957, Journal of Solar Energy, 1, 16

Dubus, G. 2006, A&A, 456, 801

Gregory, P.C. et al. 1989, ApJ, 339 1054

Gregory P.C. 2002, ApJ, 575, 427

Gregory P.C. & Neish, C. 2002, ApJ, 580, 1113

Grundstrom, E.D. et al. 2007, ApJ, 656, 437

Gupta, S. & Böttcher, M. 2006, ApJ, 650, L123

Heinz, S. & Sunyaev, R. 2002, A&A, 390, 751

Helene, 0. 1983, Nuclear Instruments & Methods 212, 319

Hillas M. 1985, Proc. of the 19th ICRC (La Jolla, USA), 3, 445

Hofmann, W. et al. 1999, Astroparticle Physics, 12, 135

Holder, J. et al.(VERITAS collaboration) 2006, Astroparticle Physics, 25, 361

Hutchings, J.B. & Crampton, D. 1981, PASP, 93, 486

Kniffen, D.A. et al. 1997, ApJ, 486, 126

Konopelko, A. 1995, Proc. of the Padova Workshop on TeV Gamma-Ray Astrophysics "Towards a Major Atmospherics Cherenkov Detector-IV, (ed. M. Cresti), Padova, Italy, 373-377

Krawczynski H. et al. 2006, Astroparticle Physics, 25, 380

Leahy, D. 2001, A&A, 318, 516

Li, T.P. & Ma, Y.Q. 1983, ApJ, 272, 317

Maier, G. et al.(VERITAS collaboration) 2007, Proc. of the 30th ICRC (Merida, Mexico), ID 700

Maier, G. et al.(VERITAS collaboration) 2007, Proc. of the 30th ICRC (Merida, Mexico), ID 810

Maraschi, L. & Treves, A. 1981, MNRAS, 194, 1

Massi, M. 2004, A&A, 422, 267

Mendelson, H. & Mazeh, T. 1989, MNRAS, 239, 733

Mirabel, I. & Rodriguez, L.F. 1994, Nature, 371, 46

Mohanty, G. et al. 1998, Astroparticle Physics, 9, 15

Neronov, A. & Chernyakova, M. 2007, MNRAS, submitted, astro-ph/0701144

Perryman, M.A.C. et al. 1997, A&A, 323, L49

Romero, G. et al. 2005, ApJ, 632, 1093

Romero, G. et al. 2007a, A&A, 474, 15

Romero, G. et al. 2007b, Proceedings of International Workshop on Clumping in Hot Stellar Winds, Potsdam, Germany [astro-ph/0708.1525]

Scargle, J.D. 1982 ApJ, 263, 835

Sidoli, L. et al. 2006, A&A, 459, 901

Smith, A. et al.(VERITAS collaboration) 2007, Proc. of the 30th ICRC (Merida, Mexico), ID 351

Steele, I.A. et al. 1998, MNRAS, 297, L5

Swanenburg, B.N. et al. 1981, ApJ, 243, L69

Taylor, A.R. & Gregory P.C. 1978, Nature, 272, 704

Taylor, A.R. & Gregory P.C. 1982, ApJ, 255, 210

Taylor, A.R. & Gregory P.C. 1984, ApJ, 283, 273

Weekes, T. et al.(VERITAS collaboration) 2002, Astroparticle Physics, 17, 221

Wen, L. et al. 2006, ApJS, 163, 372

This preprint was prepared with the AAS LaTeX macros v5.2.

Table 1. Details of the VERITAS observations of LS I +61 303.

Month	N_{Tel}[a]	Wobble offset	Elevation range	Obs. time[b] [h]	Orbital phase interval
09/2006	2	0.3°	53-61°	12.5	0.31-0.69
10/2006	2	0.3°	61-61°	7.2	0.51-0.78
11/2006	2	0.3°	54-61°	12.8	0.23-0.87
01/2007	3	0.5°	55-61°	9.9	0.41-0.76
02/2007	3	0.5°	52-57°	3.5	0.51-0.89
Total			52-61°	45.9	0.23-0.89

[a] Number of available telescopes

[b] Dead-time-corrected observation time

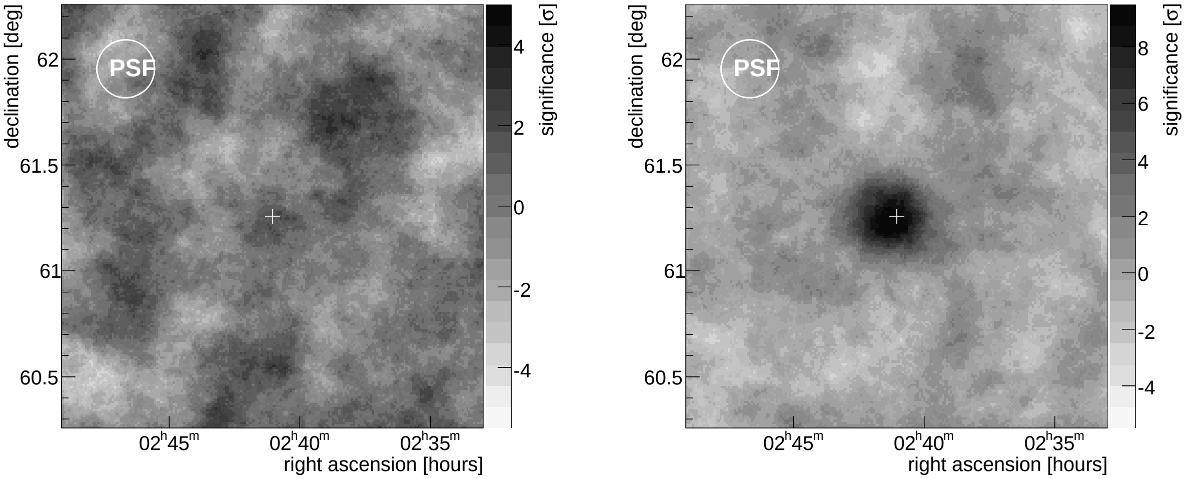

Fig. 1.— Significance map of the region around LS I +61 303 in equatorial J2000 coordinates. Left: Observations during orbital phases 0.8 to 0.5 (18.5 h of data). Right: Observations during orbital phases 0.5 to 0.8 (around apastron, 25 h of data). Significances are not corrected for number of trials. The position of the optical source (Perryman et al. 1997) is indicated by a white cross. The background is estimated using the ring-background model. Neighboring bins are correlated. Significances are calculated using the method of Li & Ma (1983), equation 17.

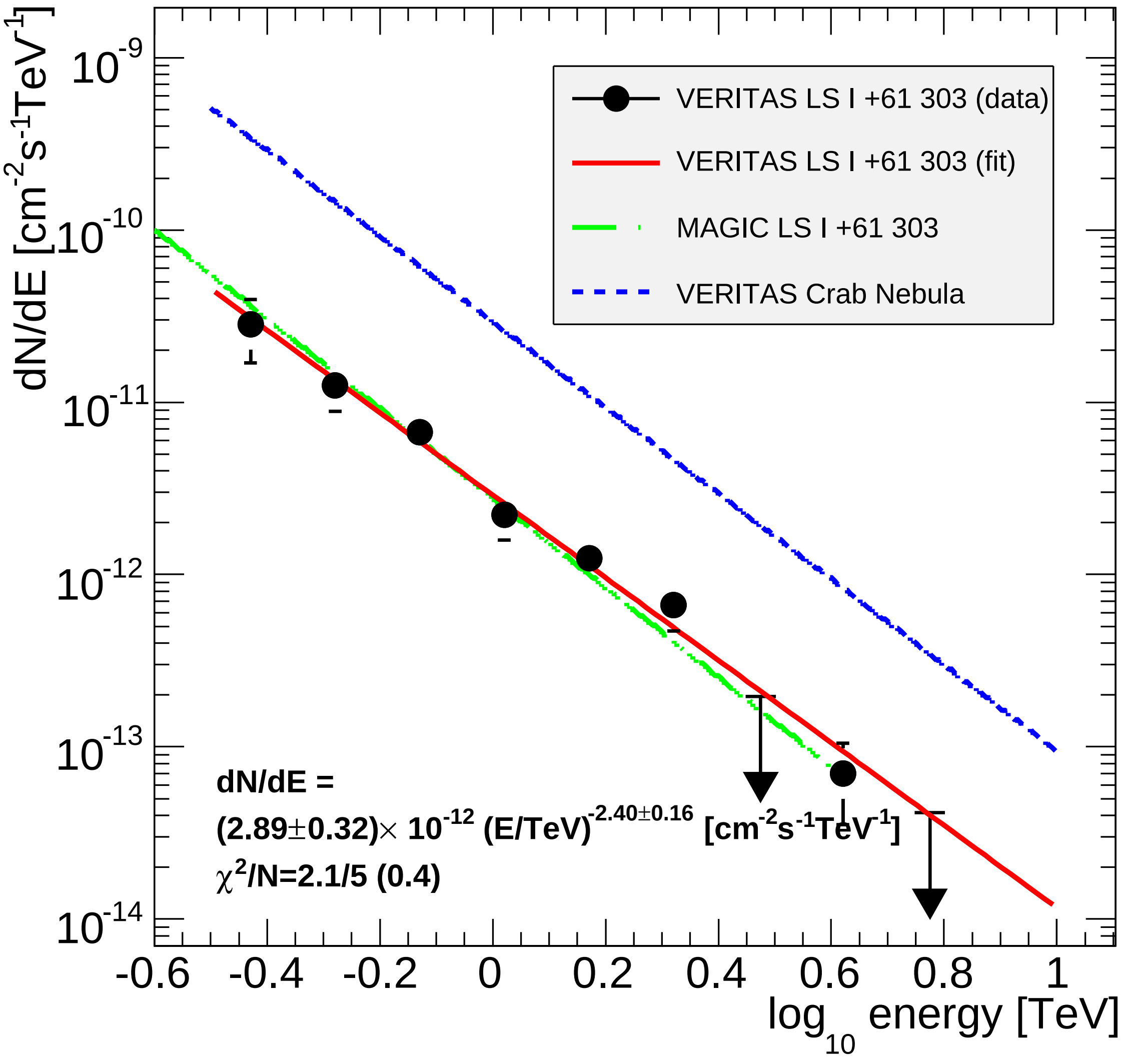

Fig. 2.— Differential energy spectrum of VHE photons above 300 GeV for LS I +61 303 around apastron (orbital phases 0.5-0.8). The markers indicate measured data points, the continuous line a fit assuming a power-law distribution of the data. Downward pointing arrows indicate upper flux limits (99% probability, Helene (1983)) for bins with significances below 2σ. For comparison, the energy distributions of LS I +61 303 published by the MAGIC collaboration for orbital phases 0.4-0.7 (Albert et al. 2006) and of the Crab Nebula measured by VERITAS (September to November 2006) (reconstructed as $\mathrm{dN/dE} = 2.85 \times 10^{-11} \cdot \mathrm{E}^{-2.49}\mathrm{cm}^{-2}\mathrm{s}^{-1}\mathrm{TeV}^{-1}$) are indicated by dotted and dashed lines, respectively.

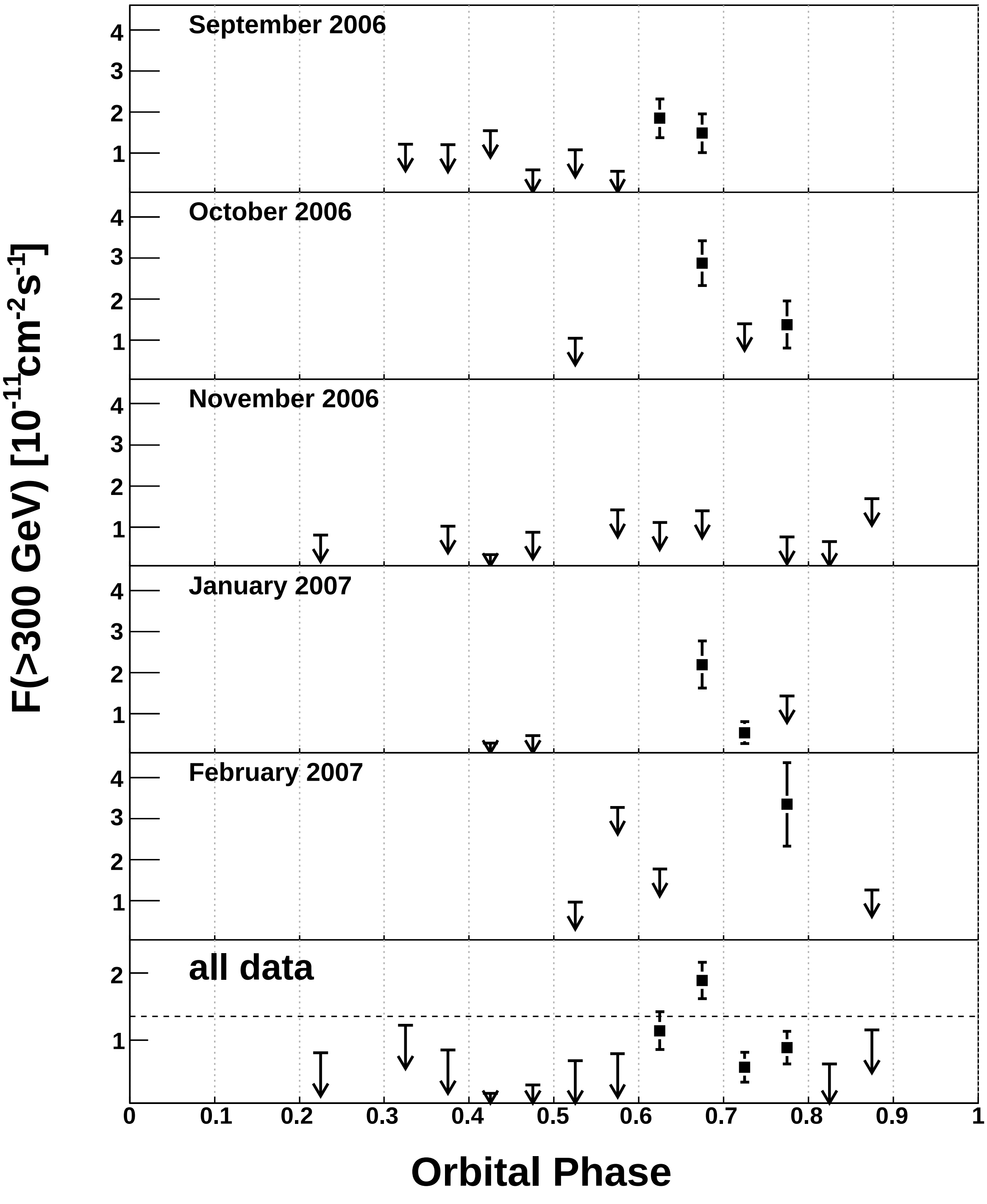

Fig. 3.— Average fluxes or upper flux limits per orbital phase bin for γ-rays with energies above 300 GeV from the direction of LS I +61 303 as a function of orbital phase. The bottom panel shows the results averaged over the whole dataset, the upper panels show the results for individual orbits. Upper flux limits (95% probability, Helene (1983)) are shown for data points with significances less than 2σ (significance calculation after Li & Ma (1983), equation 17). A flux corresponding to 10% of the flux of γ-rays from the Crab Nebula is indicated by the dashed horizontal line in the bottom panel.